analytical chemistry

pubs.acs.org/ac Article

^{13}C-Satellite Decoupling Strategies for Improving Accuracy in Quantitative Nuclear Magnetic Resonance

Adilah Bahadoor,* Andreas Brinkmann, and Jeremy E. Melanson

Cite This: *Anal. Chem.* 2021, 93, 851−858 Read Online

ACCESS | Metrics & More | Article Recommendations | Supporting Information

ABSTRACT: Quantitative ^{1}H nuclear magnetic resonance (qHNMR) with an appropriate internal standard is a well-established quantitation method for assigning purity to organic molecules. For accurate measurements, the premise of qHNMR relies on the careful selection of integrals, for both the analyte and the standard, in such a way that the selected integrals are free from interferences. The ^{13}C-satellite signals of adjacent integrals, low-level impurities, and tautomer signals are among the common integral interferences that are typically encountered. One of the simplest ways to identify and avoid these interferences is to decouple the ^{13}C-satellites. Two decoupling schemes were explored to illustrate the benefits of ^{13}C-decoupling for qHNMR or qH{^{13}C}NMR: GARP and bilevel adiabatic broadband decoupling. Unwanted sample heating and nuclear Overhauser effect (NOE) enhancements are the two main drawbacks of decoupling schemes. We show that with careful optimization of acquisition parameters and decoupling power, no excessive sample heating occurred during acquisition at 400 MHz. At 900 MHz, only bilevel adiabatic decoupling could be safely implemented. Furthermore, any undesirable NOE enhancements were completely avoided if acquisition was executed with an inverse-gated pulse sequence. We explored and confirmed the benefits of qH{^{13}C}NMR through the quantitation of a diverse set of compounds, namely, small molecules (dimethyl terephthalate and zearalenone), a ^{13}C-labeled compound ($^{13}C_6$-ochratoxin A), and an octapeptide (angiotensin II). Statistical comparisons confirmed that qH{^{13}C}NMR produced comparable data to qHNMR. However, with qH{^{13}C}NMR data providing added clarity about the presence of overlapping ^{13}C-satellites, impurities, and tautomers, it has an edge over qHNMR for accurate measurements.

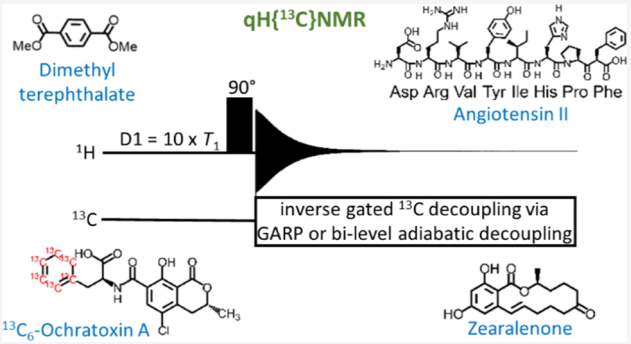

INTRODUCTION

The propensity of ^{13}C-satellites to interfere with the accurate integration of the proton nuclear magnetic resonance (NMR) signal was succinctly described for the first time by Hollis in 1963.[1] At that time, ^{13}C-decoupling pulse sequences were not yet available. With no possibility of recording proton spectra free of ^{13}C-satellites, a theoretical correction based on the natural abundance of the carbon-13 isotope was necessary to account for the interfering ^{13}C-satellite.[1] Since then, with the advent of numerous decoupling pulse sequences, recording ^{13}C-decoupled proton spectra have become a routine. By far, the most commonly employed pulse sequence to decouple ^{13}C-satellites is GARP (globally optimized alternating phase rectangular pulses).[2−7] We have employed GARP-mediated ^{13}C-decoupling to improve the accuracy of qHNMR as it efficiently prevented ^{13}C-satellite overlaps between the integrals of interest. It also easily uncovered low-level impurities (<1%) or tautomers that were concealed by ^{13}C-satellites and simplified the proton spectrum of ^{13}C-labeled compounds. This strategy worked well on simple molecules, which could be seamlessly characterized by qH{^{13}C}NMR at 400 MHz. For larger more complicated compounds such as peptides, qH{^{13}C}NMR analysis on a higher field instrument was contemplated. GARP-mediated qH{^{13}C}NMR at 900 MHz was therefore explored. Excessive heating, as immediately evident from an unstable lock signal and the presence of distorted line shapes in the proton spectrum, made it clear that an alternate approach was necessary. Adopting fundamentally new quantitative NMR methods such as quantitative carbon-13 NMR[8−12] or quantitative 2D NMR[13−22] were considered but have significant drawbacks. Both suffer from significantly extended acquisitions times. Furthermore, the quantitative 2D NMR methods require the calibration of numerous acquisition parameters to obtain reasonably accurate results. By contrast, 1D NMR experiments are easier to implement, requiring

Received: August 12, 2020
Accepted: November 30, 2020
Published: December 10, 2020

https://dx.doi.org/10.1021/acs.analchem.0c03428
Anal. Chem. 2021, 93, 851−858

optimization of few acquisition parameters such as 90° pulse lengths, relaxation delays, and acquisition times.[7,23] Therefore, to keep our quantitative NMR approach simple, we decided to explore a less demanding approach to qH{^{13}C}NMR by employing bilevel adiabatic decoupling schemes.

Bilevel adiabatic decoupling has been suggested as a viable alternative to GARP for qNMR, but concrete examples of its application for quantitative NMR purposes are rare.[24] Both decoupling methods effectively decouple ^{1}H−^{13}C signals, that is, the ^{13}C-satellites signals are not eliminated as in the DISPEL pulse sequence,[25] but rather are folded back into the main ^{1}H−^{12}C signals.[2,26,27] Cognizant of the fact that sample heating[28] and nuclear Overhauser effect (NOE) enhancements are the main drawbacks of ^{13}C-decoupling schemes, we show that both are significantly mitigated by employing long relaxation delays and minimal acquisitions times of optimal durations to avert major truncation of the free induction decay (FID). NOE build-up was completely averted when solely decoupling during acquisition. We also provide specific examples to illustrate the benefits of qH{^{13}C}NMR. Overlapping ^{13}C-satellites were prevented from interfering with integrals during the quantitation of dimethyl terephthalate and angiotensin II. Low-level impurities that would otherwise have gone undetected were exposed by qH{^{13}C}NMR when the purity of zearalenone was determined. Lastly, the tautomers of $^{13}C_6$-ochratoxin A were only identified after qH{^{13}C}NMR revealed their presence from the cover of a broad ^{1}H−^{13}C signal. More importantly, we show that unlike GARP, bilevel adiabatic decoupling was adaptable to both 400 and 900 MHz. With dimethyl terephthalate and angiotensin II as test substrates, we herein show the first successful applications of bilevel adiabatic decoupling for qH{^{13}C}NMR at 900 MHz.

EXPERIMENTAL SECTION

NMR Instrumentation. Experiments were performed using a Bruker Avance III 400 MHz spectrometer equipped with a 5 mm I.D. BBFO probe or a 900 MHz spectrometer equipped with a 5 mm I.D. room temperature triple resonance inverse TXI probe.

NMR Experimental Setup. Briefly, all samples were analyzed in triplicate at 20 °C, with a relaxation delay (D1) of 10 × T_1 and a 90° pulse angle. A minimum of 16 scans was recorded for each sample. The typical acquisition time for qHNMR was 5.4 s. For qH{^{13}C}NMR, an acquisition time of 2.5−2.7 s was the routine starting point. If truncation of the FID was observed, the acquisition time was increased accordingly, typically up to 5 s. Please see Supporting Information pg. S4 for additional information.

GARP-Mediated ^{13}C-Decoupling Procedures. The GARP-mediated qH{^{13}C}NMR was adapted from the inverse-gated Bruker pulse sequence "zgig." A 90° ^{13}C decoupling pulse length (pcpd2) of 80 μsec at 0.91 W was applied via the decoupler channel. The decoupler offset in the F2 dimension (^{13}C nucleus) was set at 80 ppm, thus enabling broadband decoupling over a sweep width of 160 ppm. Please see Supporting Information pg. S4 and Figure S1 for additional information.

Bilevel Adiabatic Decoupling Procedures. To set up bilevel adiabatic decoupling on a 400 MHz spectrometer, a high-power WURST-20 pulse (shaped pulse power: 0.79 W, duration: 1 ms, sweep width: 18 KHz or 180 ppm) and a low-power WURST-20 pulse (shaped pulse power: 0.40 W, duration: 2 ms, sweep width: 18 KHz) were implemented with a five-step phase cycle (0, 150, 60, 150, and 0°).[29] Choosing an optimal frequency offset (o2p) for each sample was best. Setting o2p close to the center of the region to be decoupled ensured that all signals within this region are subject to near-equal irradiation for complete decoupling. The 90° inverse-gated pulse sequence "zgig" was used to acquire all qH{^{13}C}NMR spectra via the WURST-20 bilevel adiabatic decoupling scheme described.

On the 900 MHz spectrometer, a high-power Chirp-32 pulse (shaped pulse power: 5.75 dB (20 W), duration: 1.5 ms, sweep width: 32 KHz or 140 ppm) and a low-power Chirp-32 pulse (shaped pulse power: 11.77 dB (5 W), duration: 3 ms, sweep width: 32 KHz) were implemented with the five-step phase cycle (0, 150, 60, 150, and 0°).[29] The Chirp-32 bilevel adiabatic decoupling scheme was implemented within a 30° inverse-gated pulse "zgig30." Please see Supporting Information pg. S4 and Figures S2 and S3 for additional information.

RESULTS AND DISCUSSION

As discussed above, ensuring high accuracy and precision in conventional qHNMR requires meticulous control of several acquisition parameters. The added complexity of GARP and bilevel adiabatic broadband decoupling required another layer of parameters to be considered and optimized. Therefore, effects such as temperature fluctuations and NOE build-up needed to be carefully studied prior to successful application of ^{13}C-decoupling procedures.

Temperature Fluctuations during Decoupling. The heating effects associated with broadband decoupling and their causative factors are a well-known phenomenon.[28,30] Nonuniform sample temperatures can distort line shapes to degrade the quality of the NMR spectrum. Relying on a variable temperature unit (VTU) to monitor sample heating is not a recommended approach as the thermocouple itself is better positioned to record the temperature of the flow gas, rather than the temperature of the section of the NMR sample under RF radiation.[28,31] To assess the extent of sample heating during decoupling, the actual temperature of 99.8% methanol-d4, commercially available from Bruker and otherwise known as the Bruker Thermometer, was recorded upon several replicate qH{^{13}C}NMR spectra recorded on that sample at a set temperature of 292.8 K (Figure 1 and Supporting Information Figure S4). On the 400 MHz NMR spectrometer, setting a temperature of 292.8 K on the VTU was the closest approximation to an actual temperature of 293.15 K (20 °C), the temperature at which all the qNMR experiments in this study were performed.

The results shown in Figure 1 emphasize that excessive sample heating is negligible whether ^{13}C-decoupling was achieved by GARP or bilevel adiabatic decoupling, as long as extended recovery delays of at least 10 × T_1 were used. The heating effects were more pronounced with a shortened relaxation delay of 1 × T_1, with up to 1.4 K increase in temperature noted during GARP decoupling. Under these same conditions, WURST-20 bilevel adiabatic decoupling outperformed GARP by inducing a minimal heating effect of about 0.4 K. This low heat output can prove advantageous for qH{^{13}C}NMR measurements of samples with high ionic strength. Aside from an unintended increase in ^{13}C-decoupling power (if incorrectly calibrated), the ionic strength of the sample is the most suitable predictor of sample heating. Samples of high ionic strength have a greater propensity to

https://dx.doi.org/10.1021/acs.analchem.0c03428
Anal. Chem. 2021, 93, 851−858

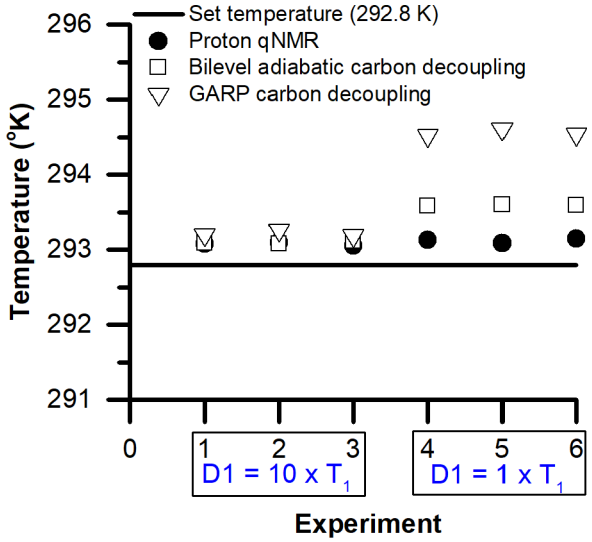

Figure 1. Actual temperature of 99.8% methanol-d4 recorded during qHNMR and qH{^{13}C}NMR at a set temperature of 292.8 K at 400 MHz over 16 recorded scans and an acquisition time of 2.7 s. With a delay of 60 s or approximately 10 × T_1 (experiments 1−3), no temperature rise of the sample was recorded. At shorter delays of 6 s or approximately 1 × T_1 (experiments 4−6), GARP decoupling causes significantly more sample heating than WURST-20 bilevel adiabatic decoupling.

absorb radio-frequency power, thus producing a heating effect.[28] Although in such cases, increasing the gas flow to mitigate temperature increases could be a viable option,[30] choosing an adiabatic pulse rather than GARP to decouple ^{13}C could on its own abates the generation of excessive heat.

Sample heating was also minimized by optimizing the acquisition time. Unlike qHNMR, where an acquisition time between 5 and 6 s was routinely used, shorter acquisitions were deemed safer for qH{^{13}C}NMR.[7] An acquisition time of 2.5−2.7 s was deemed adequate for most samples. This acquisition time produced an almost fully decayed FID (Supporting Information Figure S5), which when coupled with a recovery delay of 60 s or 10 × T_1, corresponded to a duty cycle of ∼4.3% on the decoupler. At such a low duty cycle, probe heating was effectively mitigated, subsequently resulting in reduced sample heating (Figure 1, experiments 1−3). Increasing the duty cycle to ∼43% for a 6 s delay or 1 × T_1 caused a noticeable rise in temperature of 1.4 K (Figure 1, experiments 4−6). These results underscore the importance of minimizing the duty cycle to avoid unsafe probe heating during GARP decoupling, particularly if acquisition times cannot be reduced further to prevent truncating the FID. On the other hand, the lower thermal footprint of bilevel adiabatic decoupling allows for greater flexibility in choosing shorter relaxation delays.

NOE Build-Up. In the absence of signal interferences, fully relaxed nuclei that are unaltered by NOE produce the most accurate integrals. The NOE arises from the nuclear through-space dipolar interactions. Depending on whether these interactions are between the nuclei of the same or different spin species, this is referred to as homonuclear or heteronuclear NOE, respectively. In the heteronuclear steady-state NOE, the longitudinal magnetization of one spin species, for example, ^{1}H, is enhanced or reduced if a sufficiently long, weak pulse saturates the second spin species, for example, ^{13}C. In theory, in the limit of very rapid molecular motion (extreme narrowing limit), a maximum 12% enhancement in the longitudinal ^{1}H magnetization is expected when the ^{13}C spins are saturated during an ^{1}H{^{13}C}-NMR experiment (Supporting Information Figure S6).[32] While this value rings true for an isolated two spin ^{1}H−^{13}C system, in reality, the low natural abundance of ^{13}C at 1.1% reduces the enhancement to a mere 0.13% (Supporting Information Figure S6). Negative NOEs are also possible. In a complex multispin system such as a molecule, spin relaxations can occur through multiple pathways, some of which with the potential to produce negative NOEs that reduce signal intensity.[32]

Any NOE-induced changes to the ^{1}H integrals are undesirable for qNMR and can be prevented if the spectrum is acquired employing inverse-gated ^{13}C decoupling. To counteract NOE enhancements, the timing and duration of the ^{13}C irradiation in the qNMR experimental setup are essential. These effects are demonstrated on a sample of $^{13}C_6$-tyrosine (Supporting Information Figure S7). As a ^{13}C-labeled compound, it was an appropriate model to illustrate amplified NOE transfers compared to natural abundance tyrosine. In the inverse-gated pulse sequence, ^{13}C irradiation occurs during acquisition only and typically lasts < 3 s. Coupled with long interscan delays of 10 × T_1, all NOE accumulations during acquisition effectively dissipate, preserving the true magnitude of the ^{1}H integral (Supporting Information Figure S8A). The qH{^{13}C}NMR spectrum of $^{13}C_6$-tyrosine, acquired using inverse-gated decoupling, resulted in a 0.5% integral enhancement for the four aromatic protons bonded to ^{13}C (Supporting Information Figures S7B and S9B). This perceived NOE enhancement value is not significantly different from the variation between replicate integrals typically obtained during qHNMR, which often falls in the 0.1−1% range or even higher when the integral regions are wider (Table S1). If, however, irradiation of the ^{13}C channel was continuous throughout both the delay (D1) and acquisition, the NOEs were unable to dissipate in time and accumulations occur (Supporting Information Figures S7C and S8B). Known as continuous decoupling, this experimental setup produced up to 6% enhancement in the ^{1}H integral for the aromatic protons of $^{13}C_6$-tyrosine (4 × H_B) Supporting Information Figures S7C and S9C). Similar NOE decaying patterns during inverse-gated or continuous decoupling were previously reported in the case of ^{13}C{^{1}H}-NMR.[33] As seen from Figures S7−S9, it was clear that qH{^{13}C}NMR via inverse-gated ^{13}C-decoupling could indeed provide truly quantitative integral values. It was therefore our method of choice to rely on for all the ensuing examples presented herein.

Interfering ^{13}C-Satellites in qHNMR. The ^{13}C-satellites typically represent 1.1% of the total value of the integral, matching the natural abundance of the ^{13}C isotope. While their inclusion in the integral value is optional for qualitative purposes, as a rule of thumb, integral values should incorporate the ^{13}C-satellite signals if accurate quantitation is needed. As expected, the narrower frequency dispersion of chemical shifts and the subsequent lower spectral resolution of the 400 MHz spectrometer meant that the spectra recorded at 400 MHz were more inclined to contain overlapping ^{13}C-satellites between adjacent signals than those recorded at 900 MHz. Since the majority of small molecule qHNMR work is typically performed at 400 MHz, qH{^{13}C}NMR was first explored as the alternative to eliminate overlapping ^{13}C-satellites at this frequency.

https://dx.doi.org/10.1021/acs.analchem.0c03428
Anal. Chem. 2021, 93, 851−858

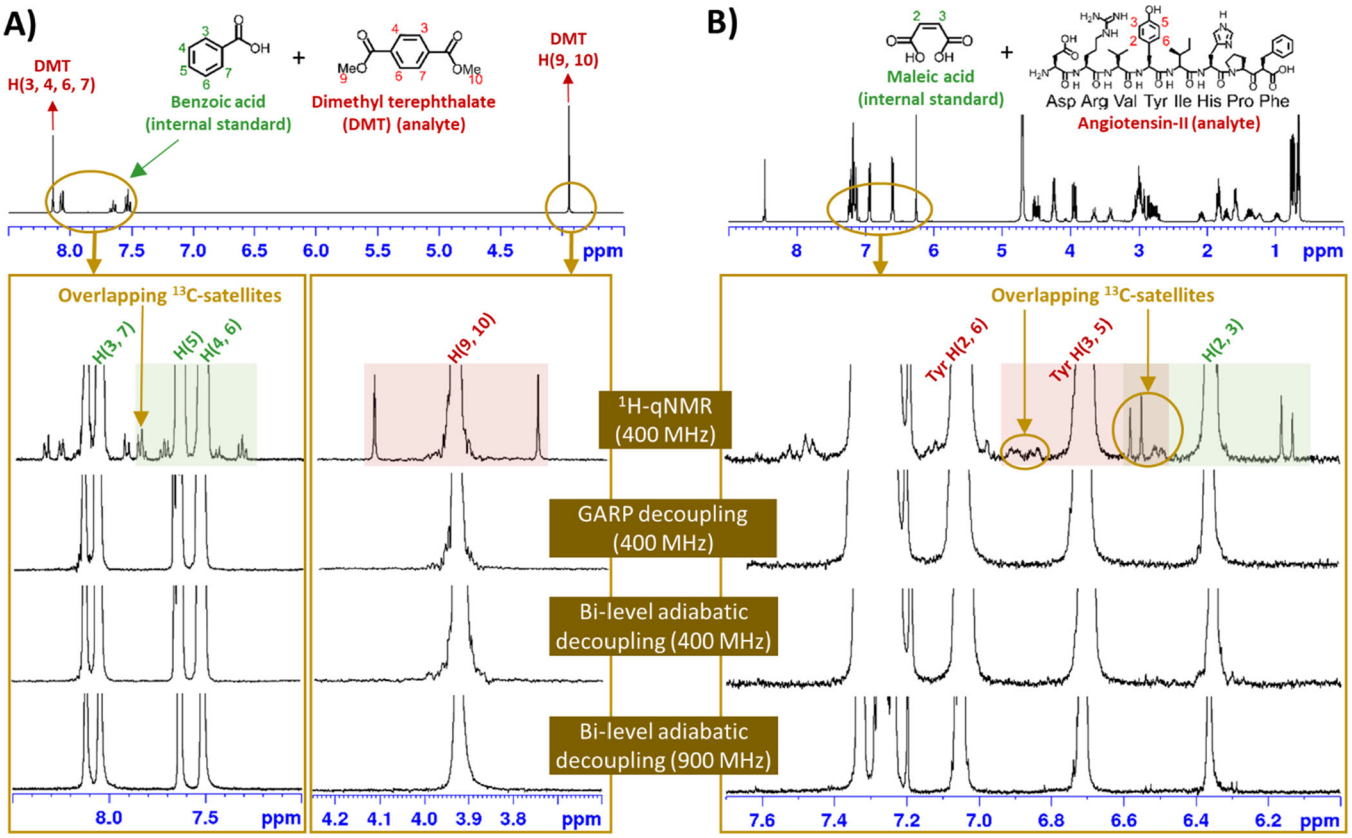

Figure 2. Overlapping ^{13}C-satellites in qHNMR. (A) A sample of dimethyl terephthalate in acetone-D_6 was analyzed with benzoic acid as the internal standard on a 400 and 900 MHz spectrometer. In the qHNMR recorded at 400 MHz, the dimethyl terephthalate integral (pink highlight) for H(9, 10) was interference-free. However, the integral region for benzoic acid, which only included H(5) + H(4, 6) (green highlight), was not. ^{13}C-satellites were not present once GARP (400 MHz only) or bilevel adiabatic (400 and 900 MHz) decoupling was performed. (B) Angiotensin II was analyzed with maleic acid as the internal standard in D_2O at 400 and 900 MHz. Both the angiotensin II integral for Tyr H(3, 5) (pink highlight) and the maleic acid integral H(2, 3) (green highlight) experienced ^{13}C-satellite interferences. Overlapping ^{13}C-satellites were of no concern with either GARP (400 MHz only) or bilevel adiabatic (400 and 900 MHz) decoupling.

To illustrate the advantages of qH{^{13}C}NMR, the ^{1}H-spectra of a small molecule, dimethyl terephthalate, and a small peptide, angiotensin II, are presented (Figure 2). For accurate quantitation, a minimum of one interference-free integral from each analyte and the standard is required. This requirement was not met from the 400 MHz qHNMR spectra of dimethyl terephthalate and angiotensin II. The qHNMR spectra of dimethyl terephthalate was recorded in the presence of benzoic acid (PS1) as the internal standard (Figure 2A). Without interference from the dimethyl terephthalate singlet at 8.12 ppm for H(3, 4, 6, 7), all five aromatic protons of benzoic acid H(3−7) would be integrated collectively as one integral. As a result of this interference, the 8.12 ppm singlet of dimethyl terephthalate and the benzoic signal for H(3, 7) at 8.05 ppm had to be discarded. The benzoic acid integral was therefore sectioned to only include H(5) and H(4, 6). Concurrently, for the dimethyl terephthalate analyte, the sharp singlet at 3.92 ppm, representing the methyl groups as positions 9 and 10, would be the integral of choice for purity calculations. One limitation of sectioning off the benzoic integral to exclude H(3, 7) was that one of its ^{13}C-satellites lined up perfectly with the ^{13}C-satellite of H(5) at 7.83 ppm (Supporting Information Figure S10). To correct this overlap, the interfering ^{13}C-satellite of H(3, 7) was subtracted from the integral encompassing H(5) + H(4, 6) before the latter was used in purity calculations (Supporting Information Figure S10 and Table S2). No integral corrections were necessary under inverse-gated ^{13}C-decoupling conditions via either GARP or WURST-20 bilevel adiabatic conditions (Figure 2A and Supporting Information Figure S11A and S11B). Recording the qHNMR spectra at 900 MHz fully resolved the overlapping ^{13}C-satellites. No complications arose in the integration of H(5) − H(4, 6) (Supporting Information Figure S12A). In this case, bilevel adiabatic ^{13}C-decoupling via Chirp-32 was performed to demonstrate feasibility at 900 MHz (Supporting Information Figure S12B). Undue sample heating was noted upon GARP decoupling as judged from distorted line shapes (data not shown). GARP-mediated ^{13}C-decoupling was not performed at 900 MHz.

As a side note, it is worth commenting on two key acquisition parameters that differed between GARP and WURST-20 bilevel adiabatic decoupling, namely, the acquisition time and the value of the center of the ^{13}C-decoupling channel. A shorter acquisition time was used for GARP (2.5 s) compared to WURST-20 bilevel adiabatic decoupling (5 s) (Supporting Information Figure S11A and S11B). Some FID truncation was apparent with an acquisition time of 2.5 s, with full decay estimated at about 4−4.5 s (data not shown). Increasing the acquisition time to hit this target was considered unsafe for the probe because of the excessive heating caused by GARP. Therefore, the acquisition time was left unchanged. On the other hand, the less demanding decoupling conditions

https://dx.doi.org/10.1021/acs.analchem.0c03428
Anal. Chem. 2021, 93, 851−858

from adiabatic pulses provided increased flexibility in adjusting the acquisition time to 5 s to fit the FID decaying profile. The value of the frequency offset "o2p" was also adjusted accordingly. While a default offset of 80 ppm for GARP decoupling was the norm for any sample, the offset was set to 95 ppm for bilevel adiabatic decoupling, the midpoint of the region in the ^{13}C-spectrum containing all relevant proton-bonded carbon atoms that needed to be decoupled (Supporting Information Figure S13). This precautionary step ensured that the benzoic acid carbon atoms positioned around 120−130 ppm and the dimethyl terephthalate peak at 52 ppm were all subjected to equal irradiation to achieve complete ^{13}C-decoupling.

The purity determination of the small peptide angiotensin II was more complicated. At 400 MHz, the qHNMR spectrum showed that there were no interference-free proton signals to integrate (Figure 2B). Any integral candidate would need to be corrected for interferences. In the end, the signal for Tyr H(3, 5) at 6.7 ppm was chosen as the most appropriate signal of angiotensin II since its interferences from two separate ^{13}C-satellite overlaps belonging to signals on its immediate flanks, namely, Tyr H(2, 6) and maleic acid H(2, 3) were clearly visible and could be corrected for (Figure 2B, Supporting Information Figure S14 and Table S3). The lone maleic acid signal for H(2, 3) was the only integral for the internal standard, which also needed to be corrected for the encroaching ^{13}C-satellite of neighboring Tyr H(3, 5). These integral corrections were unnecessary if the qH{^{13}C}NMR spectra were recorded instead. ^{13}C-decoupling via either GARP or WURST-20 bilevel adiabatic decoupling easily produced satellite-free spectra, saving the need for integral corrections (Supporting Information Figure S15A and S15B). GARP ^{13}C-decoupling at 900 MHz was not attempted on this sample as bilevel adiabatic decoupling was effective at 900 MHz (Supporting Information Figure S16A and S16B). However, to ensure uniform ^{13}C-decoupling, the frequency offset for bilevel adiabatic decoupling was set to 110 ppm. The HSQC spectra of angiotensin II with maleic acid showed that all the sp2-hybridized carbon atoms were spread in a narrow range of 115−135 ppm (Supporting Information Figure S17). By centering the frequency of the ^{13}C-decoupling channel close to this region at 110 ppm, all the relevant carbon atoms were uniformly decoupled.

Finally, to determine whether qH{^{13}C}NMR produced data comparable to qHNMR, the purity values for both dimethyl terephthalate and angiotensin II were compared by ANOVA (Table 1 and Supporting Information pgs. S30−S34). For dimethyl terephthalate, qH{^{13}C}NMR provided statistically similar results to qHNMR at both 400 and 900 MHz. The same could not be achieved for angiotensin II. With two separate integral corrections for the spectra recorded at 400 MHz, one each for Tyr H(3, 5) and MA H(2, 3), the qHNMR purity was an outlier. By judiciously avoiding integral corrections, either through ^{13}C-decoupling or by recording at a higher field (900 MHz), comparable purity values were obtained (Table 1 and Supporting Information pgs. S32−S34).

The ANOVA comparisons underscored the importance of ^{13}C-decoupling methods for complex small molecules. As an octapeptide, angiotensin II already possessed a busy ^{1}H-spectrum, further complicated by the addition of the internal standard. These cumulative complications predestined simple qHNMR acquisition at 400 MHz to produce erroneous data. While none of these complications were problematic at 900 MHz, the ANOVA assessment suggested that high field data were unnecessary if ^{13}C-decoupling methods were adopted when obtaining qNMR spectra at 400 MHz. These results highlight the seemingly improved resolution that qH{^{13}C}-NMR can provide a lower field.

Table 1. Comparison of the Purity Values of Dimethyl Terephthalate and Angiotensin II Recorded in Triplicate with and without ^{13}C-Decoupling at 400 and 900 MHz

qNMR experiment	dimethyl terephthalate purity (mg/g)	angiotensin II purity (mg/g)[a]
qHNMR (400 MHz)	999.7 ± 0.7[b]	699.7 ± 1.9[b]
qH{^{13}C}NMR (GARP decoupling—400 MHz)	999.1 ± 1.1[b]	705.8 ± 1.8[b]
qH{^{13}C}NMR (bilevel adiabatic decoupling—400 MHz)	999.3 ± 0.8[b]	707.2 ± 0.7[b]
	F (2, 6) = 0.23, p = 0.80	F (2, 6) = 28.5, p = 0.00086
qHNMR (900 MHz)	999.2 ± 0.6[b]	703.5 ± 0.8[b]
qH{^{13}C}NMR (bilevel adiabatic decoupling—900 MHz)	999.0 ± 0.5[b]	703.9 ± 0.3[b]
	F (1, 4) = 0.50, p = 0.52	F (1, 4) = 0.83, p = 0.41

[a]TFA content at nearly 25% was the major contaminant in angiotensin II.[34] [b]Uncertainty ranges are the standard deviations of triplicate analysis.

Improved Low-Level Impurity Detection. It is quite common for low-level impurities to interfere with integrals. These impurities, usually present at < 1%, can be difficult to spot, especially if they overlap with neighboring ^{13}C-satellites. The impurities most likely to interfere are those that are structurally related to the analyte as they would all share some common signal patterns emerging at similar positions in the NMR spectrum. This was the scenario encountered when the purity of zearalenone was certified by qNMR with dimethyl terephthalate as the internal standard. At first glance, the ^{1}H-spectrum did not reveal the presence of any major impurities (Figure 3). In addition, judging by the wide dispersion of signals in the region spanning 5−8 ppm, the four zearalenone

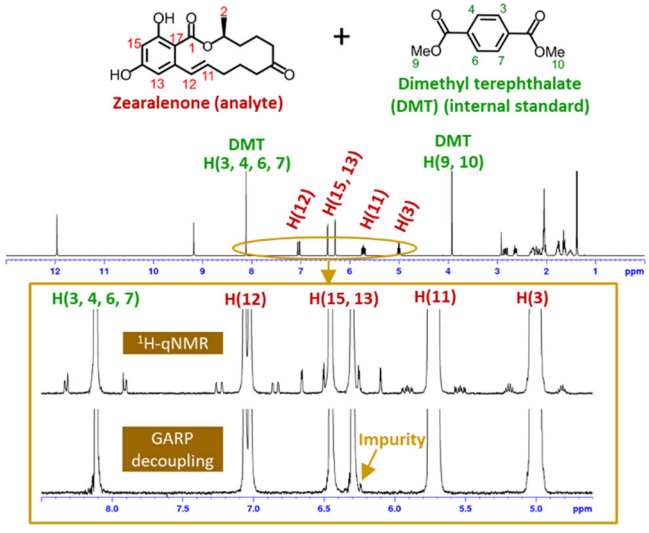

Figure 3. The purity of zearalenone was determined with dimethyl terephthalate as the internal standard at 400 MHz in acetone-d_6. GARP decoupling revealed a low-level impurity concealed by a ^{13}C-satellite in the ^{1}H-qNMR spectrum.

https://dx.doi.org/10.1021/acs.analchem.0c03428
Anal. Chem. 2021, 93, 851−858

signals for H(3), H(11), H(15, 13), and H(12) and the dimethyl terephthalate signal for H(3, 4, 6, 7) looked like good candidates for integration (Figure 3).

However, close inspection of the qH{^{13}C}NMR spectrum of zearalenone revealed a minor signal, barely emerging at a slightly lower chemical shift from the integral for H(15, 13) (Figure 3). This signal was eventually determined to stem from zearalanone, which bore strong resemblance to zearalenone, except for the lack of the double bond between C(12) and C(11) (Supporting Information Figure S18). In particular, the signals for H(15, 13) and H(3) of the two compounds overlap in the ^{1}H-spectrum. An overlay of the ^{1}H{^{13}C}-NMR spectra revealed that the ^{13}C-satellite of H(15, 13) of zearalenone completely obscured the visible part of the same signal belonging to the contaminant zearalanone (Supporting Information Figure S19). In the end, only signals for H(11) and H(12) were deemed free of interference from zearalanone and fit to use for purity calculations. To assess how the GARP-mediated qH{^{13}C}NMR matched up to qHNMR, both methods were attempted (Supporting Information Figure S20A and S20B). The bilevel adiabatic ^{13}C-decoupling procedure described above was still under exploration when this zearalenone sample was analyzed and was not performed here. An ANOVA comparison confirmed that both produced statistically similar data (Table 2 and Supporting Information pg. 35). As such, this example validates yet another versatile aspect of ^{13}C-decoupling methods for small molecules.

Table 2. Comparison of the Purity Values of Zearalenone Recorded in Triplicate at 400 MHz

qNMR experiment	purity (mg/g)	ANOVA
qHNMR	989.0 ± 1.3[a]	F (1, 4) = 2.4, p = 0.20
qH{^{13}C}NMR (GARP decoupling)	990.3 ± 0.6[a]	

[a]Uncertainty ranges are the standard deviations of triplicate analysis.

^{13}C-Satellite Decoupling for ^{13}C-Labeled Compounds and Tautomer Identification. Certified reference materials of isotopically labeled compounds provide a reliable means to produce accurate measurements when used as internal standards.[35] To produce an isotopically labeled certified reference material for $^{13}C_6$-ochratoxin A (OTAL-1), its absolute concentration was certified by qHNMR using maleic acid as the external standard.[35] However, preliminary NMR studies on the $^{13}C_6$-ochratoxin A material used to produce OTAL-1 had revealed that the material was tautomerizing in solution, due to a limited amount of material, the NMR sample would be dilute enough that ^{13}C-satellites were not likely to be visible, and lastly the ^{1}H−^{13}C signal for H(16−20) was very broad to potentially mask impurities and/or tautomers along its broad span (Figure 4). As a result of all these uncertainties, relying solely on qHNMR to obtain the concentration was not prudent. To provide a safety net, qH{^{13}C}NMR was explored as an additional option to validate the qHNMR results.

The signals for H(4, 14), H(3, 13), and H(16−20) were selected for purity calculations (Figure 4). All three signals were distinct, so signal overlap was irrelevant. The presence of interfering low-level impurities was also not a concern because this material was exhaustively purified in-house. There was however a lingering concern that the tautomerization of $^{13}C_6$-ochratoxin A was obscuring the picture. Multiple tautomers of ochratoxin A have been documented.[36,37] Our NMR experiments corroborated these reports and at the same time showed that tautomerization was minimized with CD_3OD as a solvent rather than CD_3CN + 0.1% DCOOH (Supporting Information Figure S21). Bound by the unsurmountable requirement of preparing the OTAL-1-certified reference material, the only NMR solvent that could be used for the qNMR measurement of $^{13}C_6$-ochratoxin A was CD_3CN + 0.1% DCOOH.[35] To make it work, rigorous monitoring first established that the tautomerization of $^{13}C_6$-ochratoxin A in CD_3CN + 0.1% DCOOH did not lead to unwanted decomposition pathways (Supporting Information Figure S22). Second, the location of all the relevant $^{13}C_6$-ochratoxin A tautomer signals needed to be confidently located in order to include them in their respective integral and GARP-mediated ^{13}C-decoupling helped us achieve just that. Failure to do so would lead to an underestimate of the integrals for H(4, 14), H(3, 13), and H(16−20), and concurrently, undervalue the concentration of $^{13}C_6$-ochratoxin A in the NMR sample.

The qHNMR spectra provided no help in aiding the identification of the tautomers. Site-specific ^{13}C-labeling produced a broad ^{13}C-satellite signal for H(16−20), which unbeknown was masking the $^{13}C_6$-ochratoxin A tautomers under its span. The hidden tautomers were only revealed once the broad signal was folded into a narrow peak by GARP-mediated ^{13}C-decoupling (Figure 4). Another complication arose from poor S/N from the dilute samples. It was impossible to conclusively locate the ^{13}C-satellites and the tautomers of H(3, 13) and H(4, 14) nor was it possible to distinguish between them. However, once GARP-mediated ^{13}C-decoupling was applied, the tautomer signals of H(3, 13) emerged clear from the baseline (Figure 4). The close proximity of three multiplets in the combined signal for H(4, 14) meant that while some tautomer(s) were visible, most of them were still concealed under the main peaks. However, the qH{^{13}C}NMR data provided enough evidence to conclude that the tautomer signals of H(4, 14) were following the same trend as those of H(16−20) and H(3, 13) located at slightly lower chemical shifts compared to the main signal. With this data in hand, the span of each integral region in the qHNMR could be clearly allocated to include all relevant tautomers (Figure 4). No hurdles were encountered for the qNMR data of maleic acid, which as the external standard was analyzed separately in CD_3CN + 0.1% DCOOH. Comparable bilevel adiabatic ^{13}C-decoupling data were not obtained for $^{13}C_6$-ochratoxin A as the method had not yet been adapted for qNMR purposes when these samples were quantified.

The concentrations of two independent samples of $^{13}C_6$-ochratoxin A were obtained separately by GARP-mediated qH{^{13}C}NMR and qHNMR (Table 3 and Supporting Information Figures S23 and S24). The ANOVA comparing the concentration of the two samples corroborates the results obtained by qH{^{13}C}NMR and qHNMR as statistically similar (Supporting Information pgs. S36−S39). Although the reported certified concentration for OTAL-1 was obtained by qHNMR,[35] without backup data from qH{^{13}C}NMR, these results would bear less confidence. As such, the $^{13}C_6$-ochratoxin A case study underscored the importance of ^{13}C-decoupling methods when quantifying tautomeric compounds and as a simplifying tool in the analysis and measurement of ^{13}C-labeled compounds.

https://dx.doi.org/10.1021/acs.analchem.0c03428
Anal. Chem. 2021, 93, 851−858

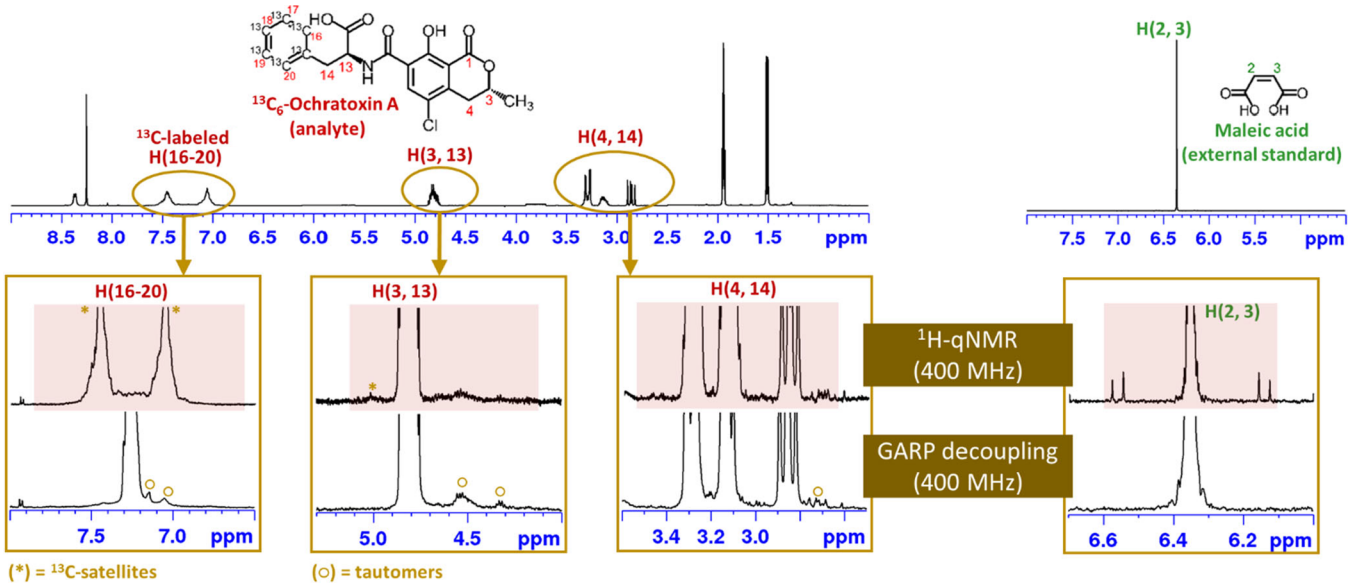

Figure 4. The concentration of $^{13}C_6$-ochratoxin A as a solution in CD_3CN + 0.1% DCOOH was obtained by qHNMR at 400 MHz with maleic acid as the external standard. $^{13}C_6$-ochratoxin A was tautomerized under these conditions. In the qHNMR spectrum, the tautomer signals were either hidden as part of the broad ^{13}C-labeled H(16−20) signal or indistinguishable from ^{13}C-satellites of H(3, 13) and H(4, 14). A roadmap to draw the boundaries of each integral region (pink highlight) of the qHNMR was obtained once all relevant tautomer signals were conclusively located by GARP-mediated qH{^{13}C}NMR.

Table 3. Concentration of Two Samples of $^{13}C_6$-Ochratoxin A Recorded at 400 MHz in Triplicate with and without ^{13}C-Decoupling

qNMR experiment	concentration of sample 1 (mg/g)	concentration of sample 2 (mg/g)
qHNMR	4.123 ± 0.039[a]	3.581 ± 0.006[a]
qH{^{13}C}NMR (GARP decoupling)	4.107 ± 0.005[a]	3.587 ± 0.010[a]
	F (1, 4) = 0.50, p = 0.52	F (1, 4) = 0.70, p = 0.45

[a]Uncertainty ranges are the standard deviations of triplicate analysis.

CONCLUSIONS

Our aim was to find an easy-to-implement alternative to qHNMR that would aid the identification of integral interferences to enhance measurement accuracy. To this end, we present data to show that ^{13}C-decoupling via either GARP or bilevel adiabatic decoupling fulfill all these requirements. The GARP decoupling scheme was easy to set up, with fixed decoupling parameters that were reliably applicable to a wide range of compounds, but was more prone to produce excessive heat, thus preventing its application at higher fields, such as 900 MHz. On the other hand, bilevel adiabatic decoupling provided an equally efficient means of decoupling ^{13}C-satellites at lower power. The fact that bilevel adiabatic decoupling was the only decoupling scheme that could be safely implemented at 900 MHz stood as a testament to its more moderate decoupling conditions and set the stage for future exploration of this method for qH{^{13}C}NMR on cryoprobes.[38] More importantly, our data suggest that when excessive corrections are required to account for integral interferences, qHNMR does not provide accurate results, as demonstrated by the 400 MHz qHNMR of angiotensin II. Recent approaches to data analysis, such as quantum mechanically calculated NMR signals, indicate a shift away from integral-based qNMR as a potential improvement to explore in conjunction with ^{13}C-decoupling methodologies.[39] Notwithstanding the availability of high field NMR instrumentation, qH{^{13}C}NMR offers the added benefit of seemingly improved resolution at lower fields. For both dimethyl terephthalate and angiotensin II, the purity values obtained by qH{^{13}C}NMR at 400 MHz were statistically equivalent to qHNMR data obtained at 900 MHz. Furthermore, by uncovering hidden impurities, tautomers, and simplifying the spectra of ^{13}C-labeled compounds, qH{^{13}C}NMR provided an added level of confidence to measurements compared to qHNMR. It is therefore highly anticipated that the results presented here will pave the way for wider adoption of qH{^{13}C}NMR as an accurate measurement tool.

ASSOCIATED CONTENT

Supporting Information

The Supporting Information is available free of charge at https://pubs.acs.org/doi/10.1021/acs.analchem.0c03428.

All supplementary figures (Figures S1 to S24), supplementary tables (Tables S1 to S3), purity calculations, and ANOVA comparisons are provided (PDF).

AUTHOR INFORMATION

Corresponding Author

Adilah Bahadoor − *Metrology, National Research Council Canada, Ottawa, Ontario K1A 0R6, Canada;* orcid.org/0000-0002-8130-5070; Email: Adilah.Bahadoor@nrc-cnrc.gc.ca

Authors

Andreas Brinkmann − *Metrology, National Research Council Canada, Ottawa, Ontario K1A 0R6, Canada;* orcid.org/0000-0001-6442-3780

Jeremy E. Melanson − *Metrology, National Research Council Canada, Ottawa, Ontario K1A 0R6, Canada*

https://dx.doi.org/10.1021/acs.analchem.0c03428
Anal. Chem. 2021, 93, 851−858

Complete contact information is available at:
https://pubs.acs.org/10.1021/acs.analchem.0c03428

Notes

The authors declare no competing financial interest.

■ ACKNOWLEDGMENTS

We thank Dr. Eriks Kupce of Bruker Corporation for helpful discussion concerning bilevel adiabatic decoupling.

■ REFERENCES

(1) Hollis, D. P. *Anal. Chem.* **1963**, *35*, 1682−1684.
(2) Shaka, A. J.; Barker, P. B.; Freeman, R. *J. Magn. Reson.* **1985**, *64*, 547−552.
(3) Meusinger, R. *Anal. Chim. Acta* **1999**, *391*, 277−288.
(4) Pauli, G. F.; Jaki, B. U.; Lankin, D. C. *J. Nat. Prod.* **2007**, *70*, 589−595.
(5) Nelson, M. A.; Bedner, M.; Lang, B. E.; Toman, B.; Lippa, K. A. *Anal. Bioanal. Chem.* **2015**, *407*, 8557−8569.
(6) Soininen, P.; Haarala, J.; Vepsäläinen, J.; Niemitz, M.; Laatikainen, R. *Anal. Chim. Acta* **2005**, *542*, 178−185.
(7) Pauli, G. F.; Jaki, B. U.; Lankin, D. C. *J. Nat. Prod.* **2005**, *68*, 133−149.
(8) Freeman, R. H.; Kaptein, R. *J. Magn. Reson.* **1972**, *7*, 327−329.
(9) Shoolery, J. N. *Prog. Nucl. Magn. Reson. Spectrosc.* **1977**, *11*, 79−93.
(10) Cookson, D. J. S.; E, B. *J. Magn. Reson.* **1984**, *57*, 355−368.
(11) Otte, D. A.; Borchmann, D. E.; Lin, C.; Weck, M.; Woerpel, K. A. *Org. Lett.* **2014**, *16*, 1566−1569.
(12) Mäkelä, A. V. K.; Heikkinen, S. *J. Magn. Reson.* **2010**, *204*, 124−130.
(13) Martineau, E. G. P.; Tea, I.; Akoka, S. *J. Pharm. Biomed. Anal.* **2011**, *54*, 252−257.
(14) Martineau, E. T. I.; Akoka, S.; Giraudeau, P. *NMR Biomed.* **2012**, *25*, 985−992.
(15) Giraudeau, P. *Magn. Reson. Chem.* **2014**, *52*, 259−272.
(16) Koskela, H. V. T. *Magn. Reson. Chem.* **2002**, *40*, 705−715.
(17) Heikkinen, S. T.; M, M.; Karhunen, P. T.; Kilpeläinen, I. *J. Am. Chem. Soc.* **2003**, *125*, 4362−4367.
(18) Koskela, H. K. I.; Heikkinen, S. *J. Magn. Reson.* **2005**, *174*, 237−244.
(19) Zhang, L. G. *Magn. Reson. Chem.* **2007**, *45*, 37−45.
(20) Fardus-Reid, F.; Warren, J.; Le Gresley, A. *Anal. Methods* **2016**, *8*, 2013−2019.
(21) Koskela, H. H. O.; Kilpeläinen, I.; Heikkenen, S. *J. Magn. Reson.* **2010**, *202*, 24−33.
(22) Koskela, H. *Annu. Rep. NMR Spectrosc.* **2009**, *66*, 1−31.
(23) Pauli, G. F.; Chen, S. N.; Simmler, C.; Lankin, D. C.; Godecke, T.; Jaki, B. U.; Friesen, J. B.; McAlpine, J. B.; Napolitano, J. G. *J. Med. Chem.* **2014**, *57*, 9220−9231.
(24) Pauli, G. F. G. T.; Jaki, B. U.; Lankin, D. C. *J. Nat. Prod.* **2012**, *75*, 834−851.
(25) Moutzouri, P.; Kiraly, P.; Phillips, A. R.; Coombes, S. R.; Nilsson, M.; Morris, G. A. *Anal. Chem.* **2017**, *89*, 11898−11901.
(26) Kupce, E. F. R.; Wider, G.; Wuthrich, K. *J. Magn. Reson. Series A* **1996**, *122*, 81−84.
(27) Kupče, E. *J. Magn. Reson.* **2020**, *318*, 106799.
(28) Wang, A. C. B. A. *J. Biomol. NMR* **1993**, *3*, 715−720.
(29) Tycko, R. P. A.; Gluckheimer, R. *J. Chem. Phys.* **1985**, *83*, 2775−2802.
(30) Loening, N. M. K. J. *J. Magn. Reson.* **2002**, *159*, 55−61.
(31) Bruker, Variable Temperature Control for NMR Probes User Manual. Version 002. 2012 11−30.
(32) Claridge, T. D. W., Correlations Through Space: The Nuclear Overhauser Effect. In *High-Resolution NMR Techniques in Organic Chemistry*, 2nd ed.; Elsevier: 2009; 315−380.
(33) Reich, H. J. The Nuclear Overhauser Effect. https://www.chem.wisc.edu/areas/reich/nmr/08-tech-02-noe.htm (accessed March 30, 2020).
(34) Melanson, J. E.; Thibeault, M.-P.; Stocks, B. B.; Leek, D. M.; McRae, G.; Meija, J. *Anal. Bioanal. Chem.* **2018**, *410*, 6719−6731.
(35) Bates, J.; Bahadoor, A.; Cui, Y.; Meija, J.; Windust, A.; Melanson, J. E. *J. AOAC Int.* **2019**, *102*, 1756−1766.
(36) Frenette, C.; Paugh, R. J.; Tozlovanu, M.; Juzio, M.; Pfohl-Leszkowicz, A.; Manderville, R. A. *Anal. Chim. Acta* **2008**, *617*, 153−161.
(37) Dais, P.; Stefanaki, I.; Fragaki, G.; Mikros, E. *J. Phys. Chem. B* **2005**, *109*, 16926−16936.
(38) de Graaf, R. A.; Chowdhury, G. M. I.; Behar, K. L. *Anal. Chem.* **2014**, *86*, 5032−5038.
(39) Choules, M. P.; Bisson, J.; Gao, W.; Lankin, D. C.; McAlpine, J. B.; Niemitz, M.; Jaki, B. U.; Franzblau, S. G.; Pauli, G. F. *J. Org. Chem.* **2019**, *84*, 3055−3073.